Supporting Information

Tuning the Performance of Zinc Hexacyanoferrate Cathodes via Ferrocyanide/Ferricyanide Precursor Selection for High-Efficiency Zinc-Ion Storage

Jiayao Wang,[a] Zewei Hu,[a] Qingqing Zheng,[a] Xin Wang,[a] Haiying Lu,[a] Yuju Qi,[a] Fuliang Chen,[a] Chao Han,[b] Chandrasekar M Subramaniyam,[c] Weijie Li*[a]

1. Experimental Section

Materials Synthesis:

All materials in this work are of analytical grade and have not undergone further purification. K_3 was prepared by a co-precipitation method at room temperature. Typically, Solution A was made by dissolving 3 mmol $ZnSO_4 \cdot H_2O$ in 20 mL deionized water. Solution B was made by dissolving 2 mmol $K_3Fe(CN)_6$ in 20 mL deionized water. Then, solution A was added dropwise to solution B water under constant stirring. After stirring at room temperature for 4 hours, the precipitate was centrifuged with deionized water and anhydrous ethanol and then vacuum-dried at 80 ℃ for 12 hours. The synthesis of Na_4 and K_4 followed the same procedure as that of K_3, except that $K_3Fe(CN)_6$ was replaced by equal amounts of $Na_4Fe(CN)_6$ and $K_4Fe(CN)_6$.

Material Characterization:

X-ray diffraction (XRD) was performed using a Bruker D8 (Cu Kα radiation). Water content was determined by Thermogravimetric analysis (TG 209 F1 Libra), while the element composition was obtained by ICP-OES (SPECTRO BLUE). The microstructure was examined via Scanning electron microscopy (SEM, JEOL JSM-7100F) with an energy dispersive X-ray spectrometer (EDS). The valence states were analyzed by X-ray photoelectron spectroscopy (XPS) with a Thermo Fisher Scientific Escalab 250 Xi. The Raman spectra were collected from a Raman spectrometer (Renishaw in Via) using an excitation wavelength of 532 nm.

Electrochemical Measurements:

The working electrode was composed of 70 wt% active materials (K_3, Na_4, K_4), 20 wt% Ketjen black and 10 wt% polytetrafluoroethylene. The mixture was ground for 30 minutes to form a suitable consistency slurry. The slurry was evenly applied onto a 10 mm-diameter circular graphite foil and then dried under vacuum at 80 °C for 12 hours. A zinc foil was used as anode. The electrolyte for electrochemical performance test was 3 M $Zn(CF_3SO_3)_2$. The CR2032 coin-type battery was manufactured by assembling the electrodes, separator, and electrolyte in the air environment. All

assembled cells were left to stand for 6 h before testing. A Neware battery test system (CT-4008Tn-5V10mA-HWX, Shenzhen, China) was used to evaluate the electrochemical performance of the cells. Galvanostatic charge/discharge (GCD) measurements were carried out within the voltage range of 0.7~1.9 V (vs. Zn^{2+}/Zn). For anode-less battery, zinc-deposited copper was used as the anode, with a deposition current of 1 mA/cm^2. Cyclic voltammetry (CV) and electrochemical impedance spectroscopy (EIS) were conducted using a Gamry Interface 1010E electrochemical workstation. The frequency range of EIS was 0.01 Hz to 100000 Hz. The galvanostatic intermittent titration technique (GITT) testing was conducted at a specific current of 20 mA g^{-1}, in which the cell was alternately charged/discharged for 600 s followed by 3600 s of rest. The Zn^{2+} diffusion coefficient can be calculated using the equation: $D = \frac{4}{\pi\tau}(\frac{m_B V_M}{M_B S})^2(\frac{\Delta E_s}{\Delta E_t})^2$, where m_B, V_M, and M_B represent the mass, molar volume, and molar mass of the active materials; τ is the testing time in each step; S is the electrode contact area; ΔE_s is the voltage change before and after the titration; and ΔE_t is the voltage change during the titration.

Computational method:

Density functional theory (DFT) calculations were performed using the Vienna Ab initio Simulation Package (VASP), which employs a plane-wave basis set and the projector augmented wave (PAW) method. The Perdew-Burke-Ernzerhof (PBE) exchange-correlation functional within the generalized gradient approximation (GGA) was used. Atomic positions were fully relaxed until the forces on all atoms were below 0.05 eV/Å, with an electronic iteration convergence criterion of 10^{-5} eV. The plane-wave kinetic energy cutoff was set to 520 eV. Brillouin zone integrations were performed using a Gamma-centered k-points mesh with density of about 0.03 Å^{-1}. The diffusion barriers were calculated using the climbing image nudged elastic band (CI-NEB) method.

2. Supplementary Figures

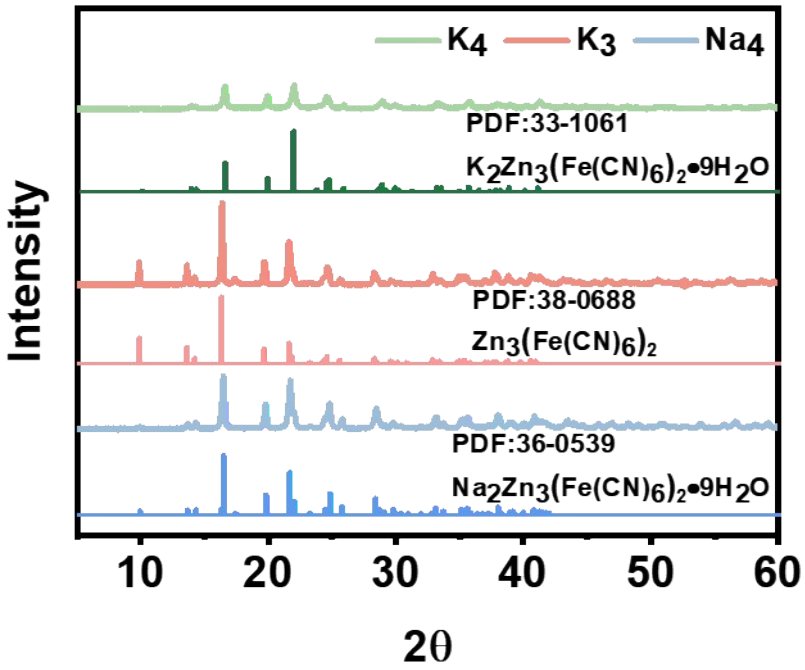

Figure S1. XRD pattern of Na_4, K_3, and K_4.

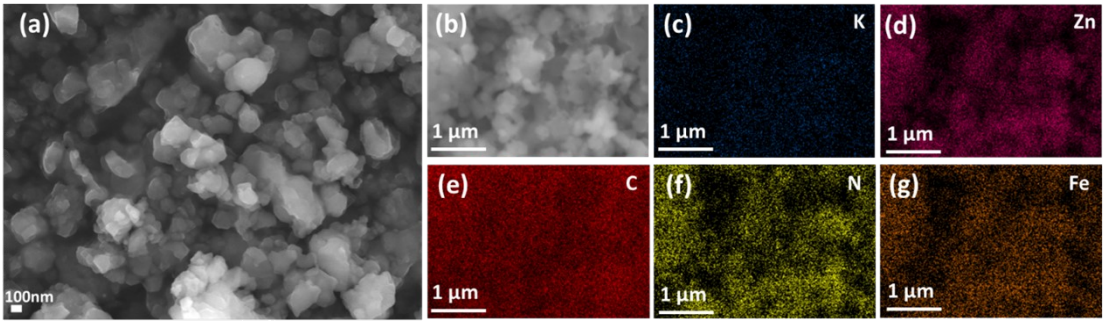

Figure S2. SEM images of K_3 and corresponding elemental mapping images.

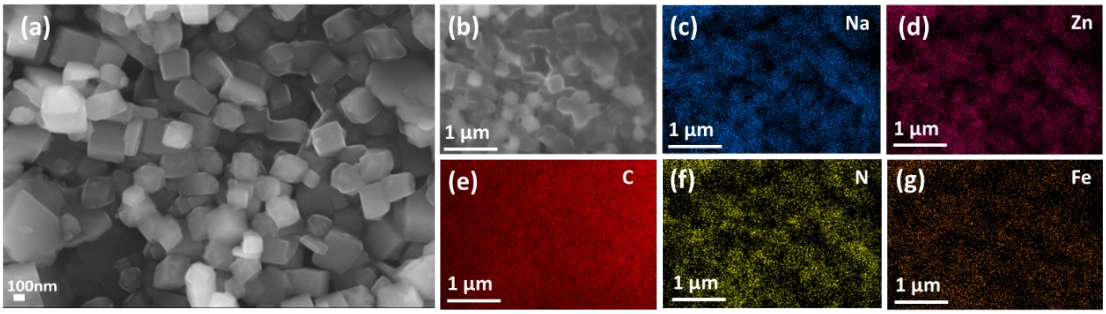

Figure S3. SEM images of Na_4 and corresponding elemental mapping images.

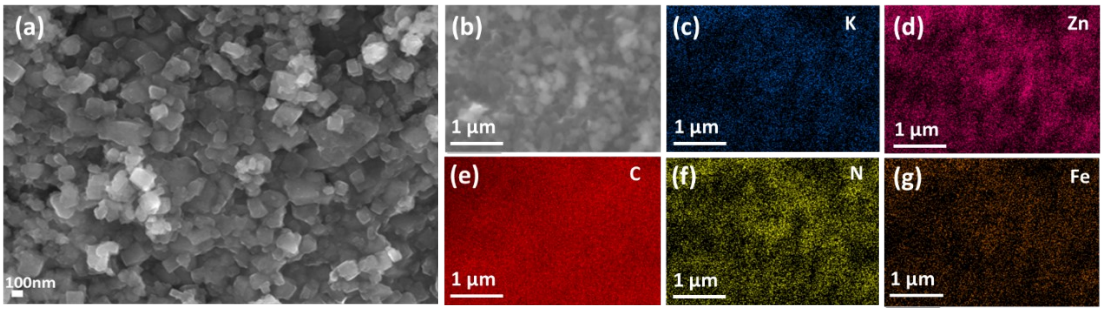

Figure S4. SEM images of K_4 and corresponding elemental mapping images.

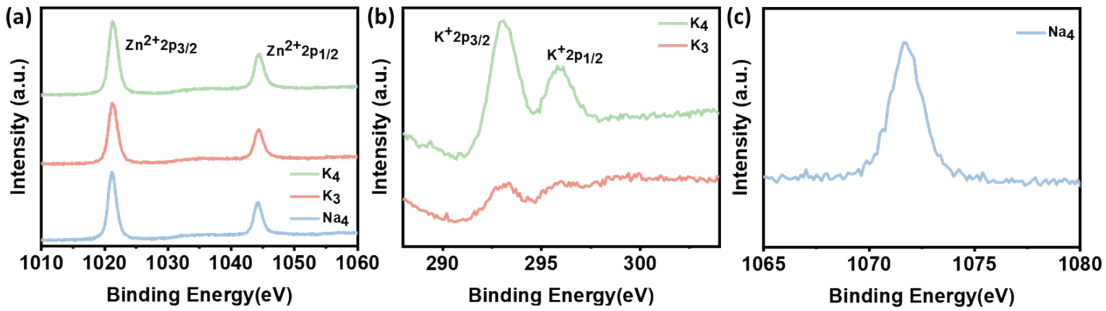

Figure S5. (a) Zn 2p XPS spectra of Na_4, K_3, and K_4. (b) K 2p XPS spectra of K_3 and K_4. (c) Na 1s XPS spectra of Na_4.

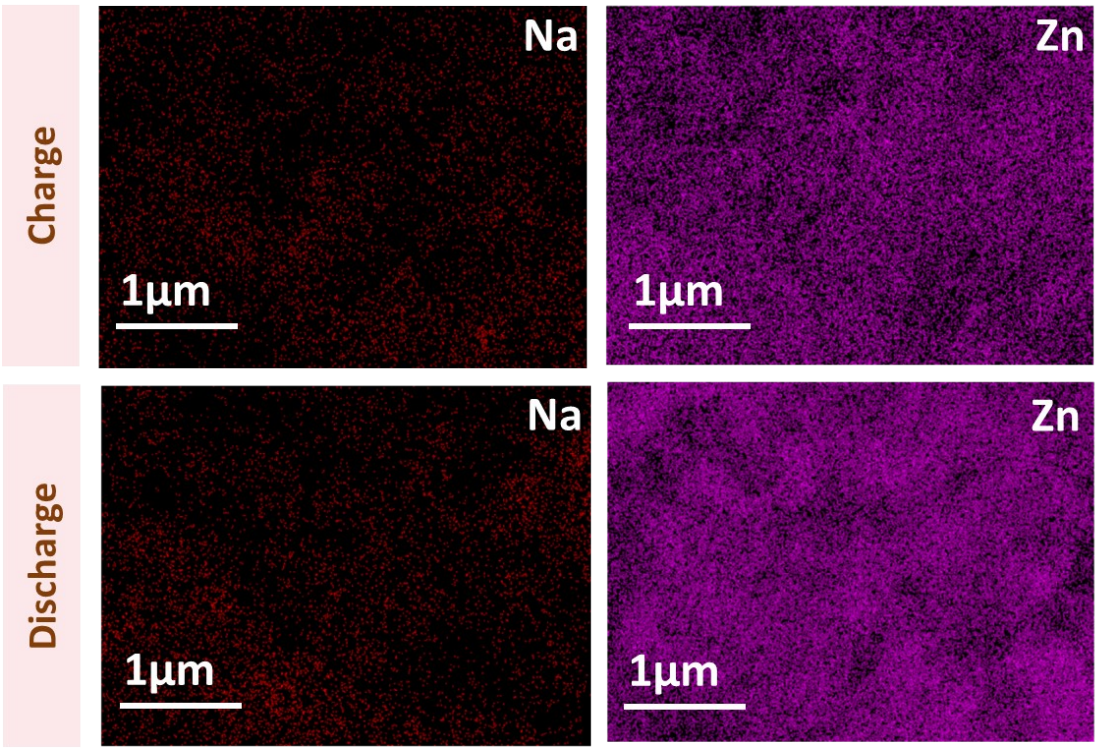

Figure S6. Elemental mapping images of Na_4 under the states of first-cycle charge and first-cycle charge-discharge.

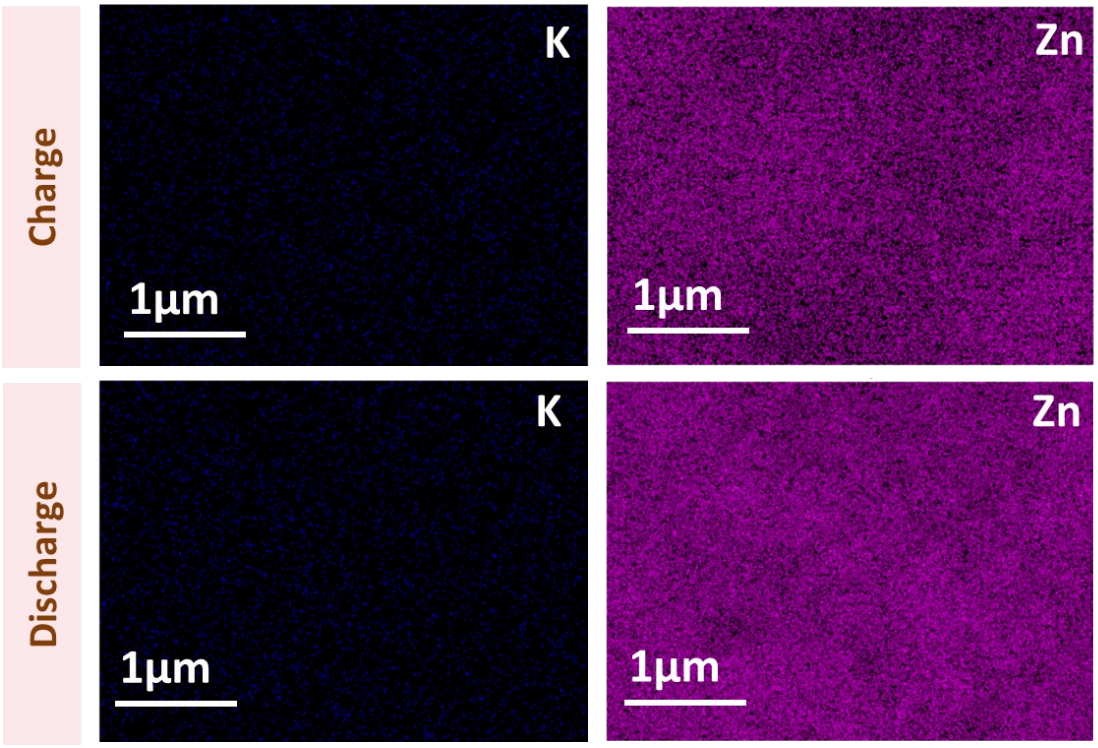

Figure S7. Elemental mapping images of K_4 under the states of first-cycle charge and first-cycle charge-discharge.

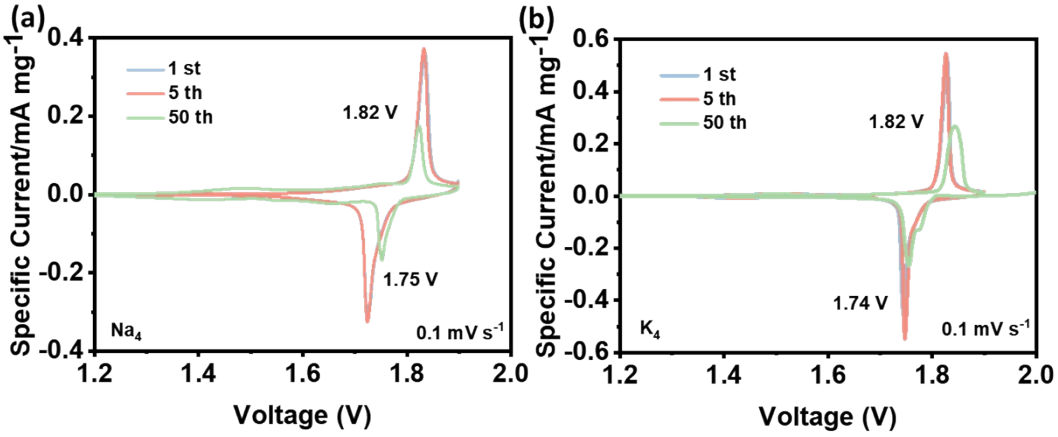

Figure S8. CV curves of (a) Na_4 and (b) K_4.

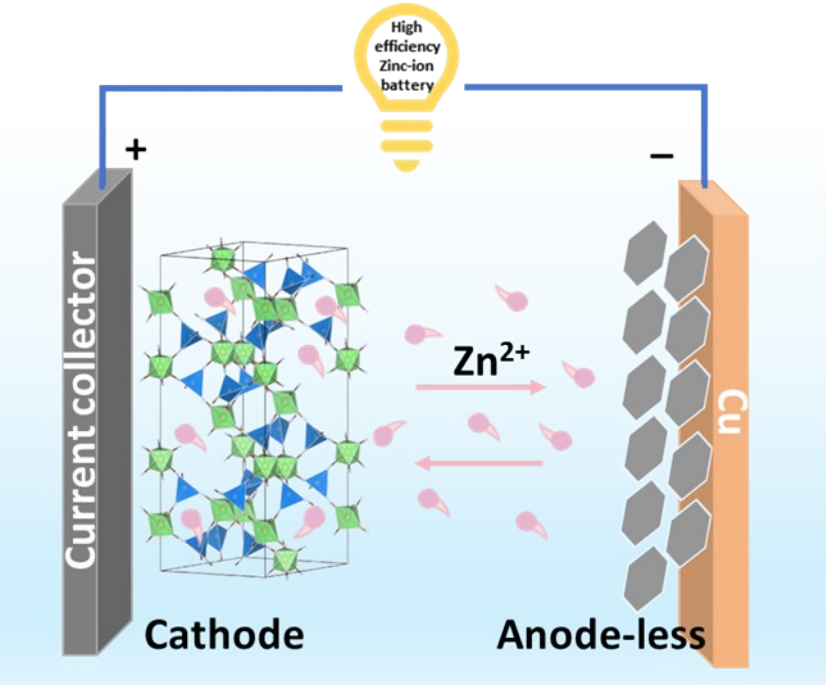

Figure S9. Schematic illustration of the Anode-less battery.

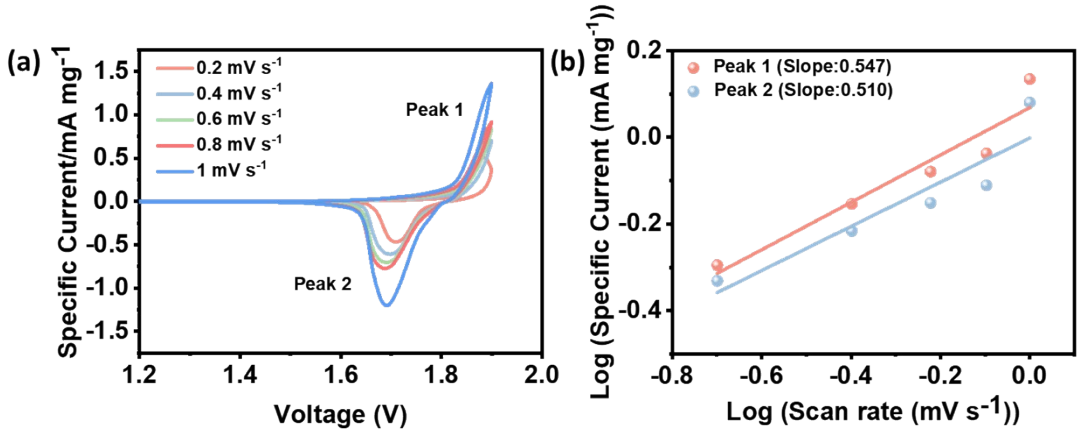

Figure S10. (a) CV curves at different scan rates from 0.2 to 1 mV s^{-1} of Na_4 and (b) the corresponding linear fitting of log (i) and log (v) plots.

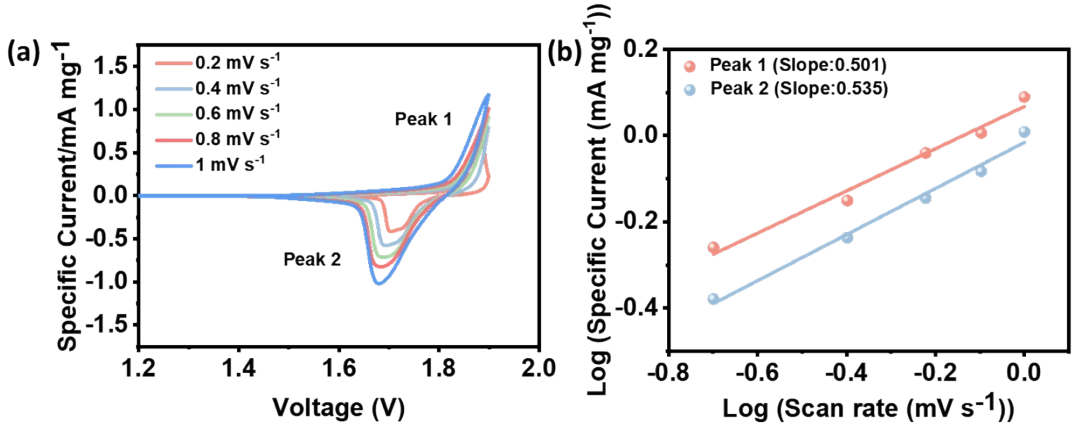

Figure S11. (a) CV curves at different scan rates from 0.2 to 1 mV s^{-1} of K_4 and (b) the corresponding linear fitting of log (i) and log (v) plots.

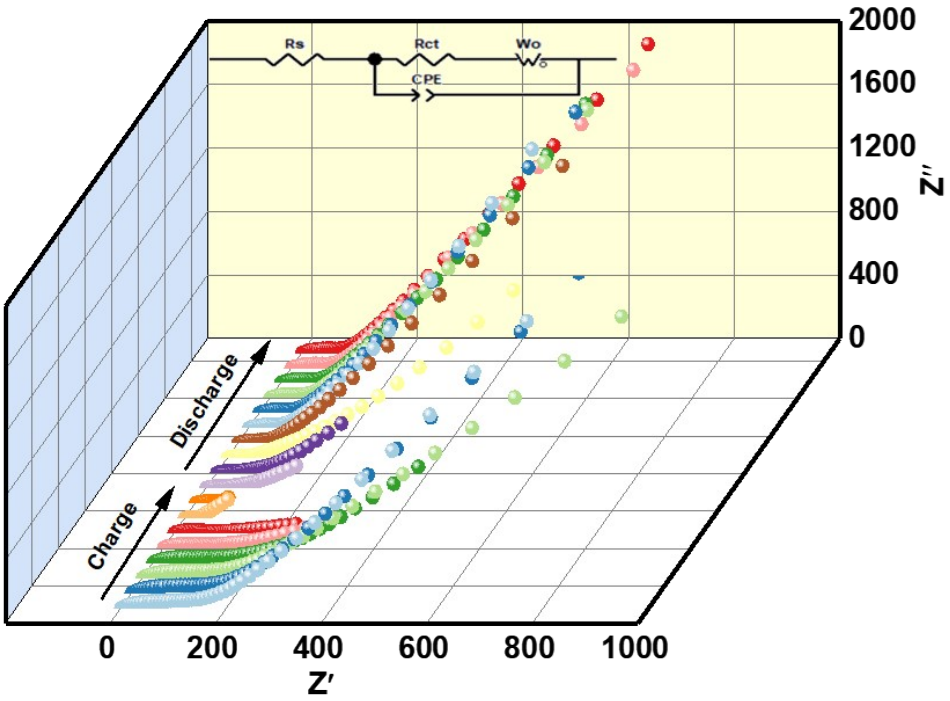

Figure S12. In-situ EIS curves of Na_4.

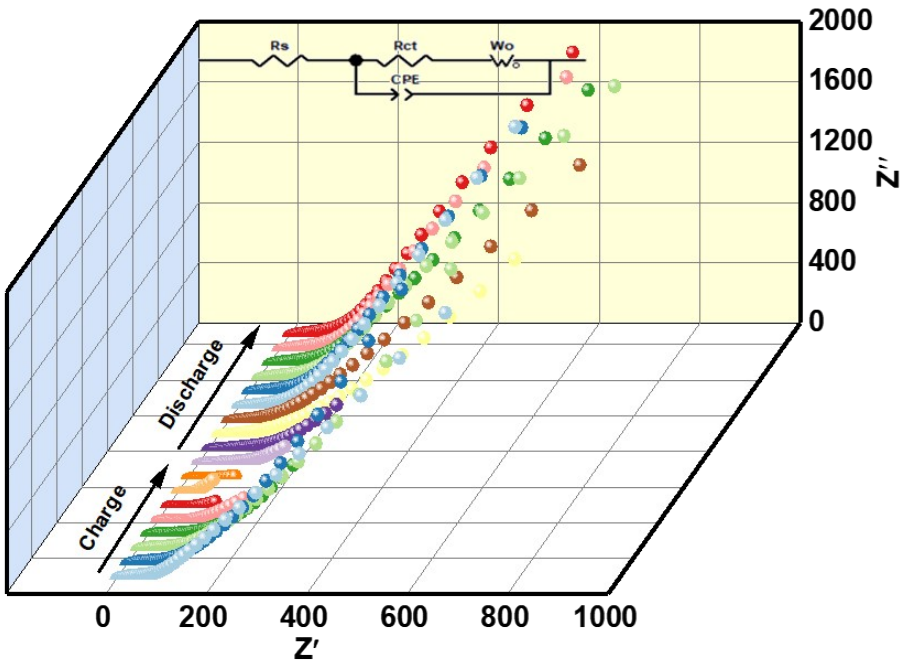

Figure S13. In-situ EIS curves of K_4.

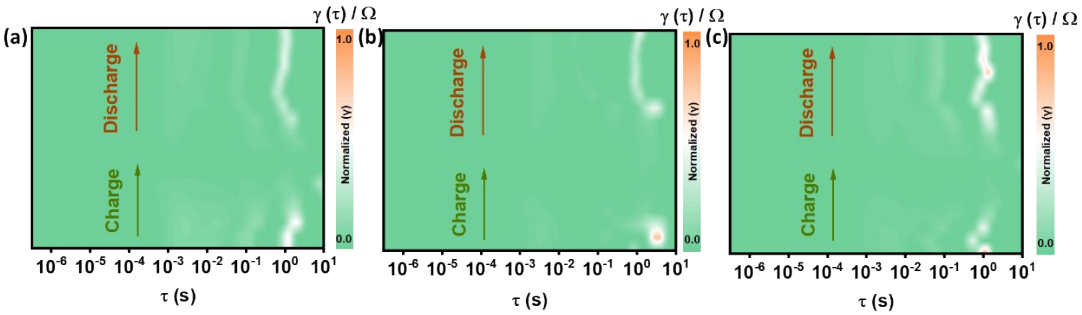

Figure S14. DRT results of (a) Na_4, (b) K_3, and (c) K_4.

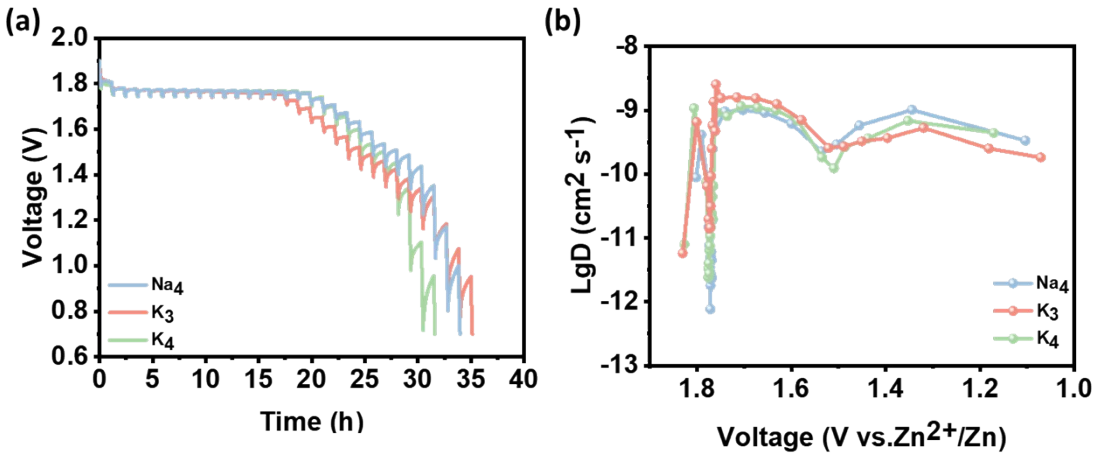

Figure S15. (a) GITT curves and (b) the calculated Zn^{2+} diffusion coefficients.

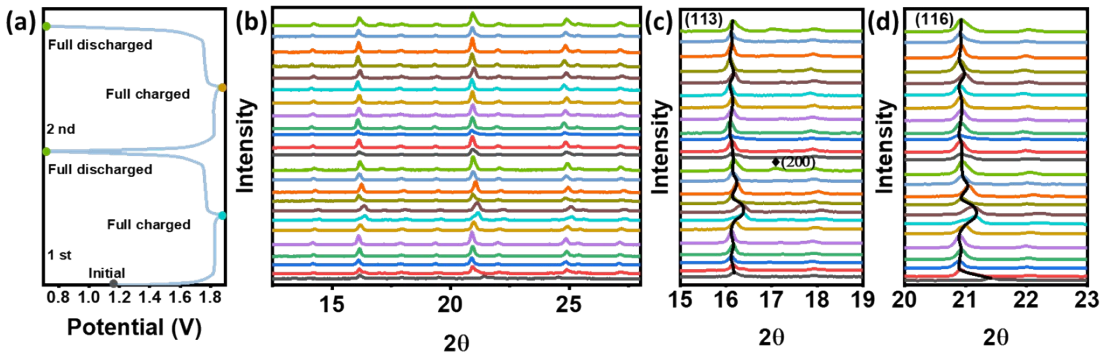

Figure S16. (a) GCD curve and (b-d) ex-situ XRD patterns of Na_4 at different states during the first two cycles.

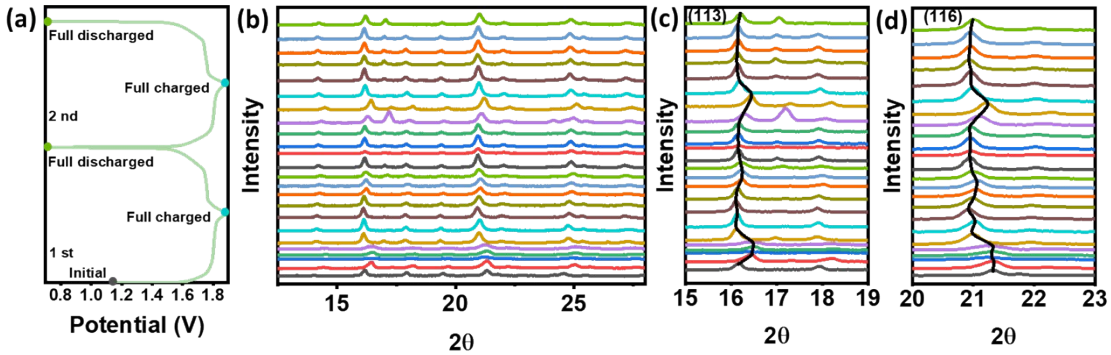

Figure S17. (a) GCD curve and (b-d) ex-situ XRD patterns of K_4 at different states during the first two cycles.

Supplementary Tables

Table S1. Detailed structural information of the Na_4 sample after Rietveld refinement.

Na_4. Space group R-3c, a=b=12.47846 Å, c=32.95311 Å, and α=β=90°, γ=120°, V= 4443.744 Å^3. R_{wp}=6.1%.			
Atom	x	y	z
Na1	0.3504	0.30629	0.3
Zn1	0.29063	0	0.25
Fe1	0	0	0.14802
C1	-0.01939	0.18106	1
C2	0.21481	0.21714	1
N1	-0.02356	0.20625	1
N2	0.14385	0.23694	1
O1	0.23177	0.28654	0.17
O2	0.2441	0.34011	0.15
O3	0.39194	0.31611	0.28
O4	0.36215	0.30109	0.56
O5	0.3102	0.2774	0.4

Table S2. Detailed structural information of the K_3 sample after Rietveld refinement.

K_3. Space group R-3c, a=b=12.54776 Å, c=32.83652 Å, and α=β=90°, γ=120°, V=4477.343 Å^3. R_{wp}=9.06%.			
Atom	x	y	z
Zn1	0	0.29511	0.75
Fe1	0	0	0.14695
C1	0.02613	0.90449	0.18158
C2	0.01369	0.13415	0.37143
N1	0.04525	0.23969	0.71889

N2	0.30649	0.1576	0.47716

Table S3. Detailed structural information of the K_4 sample after Rietveld refinement.

K_4. Space group R-3c, a=b=12.57255 Å, c= 32.14694 Å, and α=β=90°, γ=120°, V=4400.653 Å^3. R_{wp}=6.55%.

Atom	x	y	z
K1	0.0188	0.20324	0.05928
Zn1	0.28567	0	0.25
Fe1	0	0	0.14675
C1	-0.00338	0.11652	0.17089
C2	0.14614	0.11962	0.11765
N1	0.06681	0.31386	0.22495
N2	0.2245	0.02418	0.01633
O1	0.40424	0.01171	0.04176
O2	0.22486	0.02204	0.00734
O3	0.07463	-0.03409	0.01506

Table S4. Mass ratio of each atom in Na_4, K_3 and K_4 obtained by ICP-OES and elemental analysis.

Samples	Elements	Weight (wt.%)	Atomic ratio	Chemical formula
Na_4	Na	4.58	0.83	$Na_{0.83}Zn_{1.5}Fe(CN)_6 \cdot 4.29H_2O$
	Zn	23.8	1.5	
	Fe	13.2	1	
K_3	K	0.97	0.1	$K_{0.1}Zn_{1.54}Fe(CN)_6 \cdot 1.95H_2O$
	Zn	26.4	1.54	
	Fe	14.7	1	
K_4	K	7.44	0.79	$K_{0.79}Zn_{1.54}Fe(CN)_6 \cdot 3.63H_2O$
	Zn	24.5	1.54	
	Fe	13.3	1	

Table S5. Comparison of Key Characteristics of Na_4, K_3, and K_4.

Key Characteristics	Na_4	K_3	K_4
Crystal structure	R-3c	R-3c	R-3c
Alkali metal ion content (per formula unit)	$Na^+ = 0.83$	$K^+ = 0.1$	$K^+ = 0.79$
Crystalline water content (%)	19.00	10.01	16.09
Fe valence state	Fe^{2+} (single valence)	Fe^{2+}/Fe^{3+} (mixed valence)	Fe^{2+} (single valence)
Rate capacity (mAh g^{-1}, 1000 mA g^{-1})	22	35	33
Capacity retention	/	70.5	/

after 800 cycles (%)			
Zn^{2+} migration aenergy barrier (eV)	1.46	0.65	1.30
Phase transition during cycling	Irreversible (monoclinic phase)	Reversible (no phase change)	Irreversible (monoclinic phase)